



Technical Note

# Monitoring of Wheat Powdery Mildew under Different Nitrogen Input Levels Using Hyperspectral Remote Sensing

Wei Liu <sup>1</sup>, Chaofei Sun <sup>1</sup>, Yanan Zhao <sup>1,2</sup>, Fei Xu <sup>1,3</sup>, Yuli Song <sup>3</sup>, Jieru Fan <sup>1,\*</sup>, Yilin Zhou <sup>1</sup> and Xiangming Xu <sup>4</sup>

<sup>1</sup> State Key Laboratory for Biology of Plant Diseases and Insect Pests, Institute of Plant Protection, Chinese Academy of Agricultural Sciences, Beijing 100193, China; wliusdau@163.com (W.L.); sunchaofei1992@163.com (C.S.); zyanan1225@163.com (Y.Z.); 13623832653@163.com (F.X.); ylzhou@ippcaas.cn (Y.Z.)

<sup>2</sup> College of Agriculture and Forestry Science and Technology, Hebei North University, Zhangjiakou 075000, China

<sup>3</sup> Key Laboratory of Integrated Pest Management on Crops in Southern Part of North China, Institute of Plant Protection, Henan Academy of Agricultural Sciences, Ministry of Agriculture and Rural Affairs of China, Zhengzhou 450002, China; songyuli2000@126.com

<sup>4</sup> NIAB EMR, New Road, East Mallang, Kent ME19 6BJ, UK; Xiangming.Xu@emr.ac.uk

\* Correspondence: fanjieru1981@126.com

**Abstract:** Both wheat powdery mildew severities and nitrogen input levels can lead to changes in spectral reflectance, but they have been rarely studied simultaneously for their effect on spectral reflectance. To determine the effects and influences of different nitrogen input levels on monitoring wheat powdery mildew and estimating yield by near-ground hyperspectral remote sensing, Canopy hyperspectral reflectance data acquired at Feekes growth stage (GS) 10.5.3, 10.5.4, and 11.1 were used to monitor wheat powdery mildew and estimate grain yield under different nitrogen input levels during the 2016–2017, 2017–2018, 2018–2019 and 2019–2020 seasons. The relationships of powdery mildew and grain yield with vegetation indices (VIs) derived from spectral reflectance data across the visible (VIS) and near-infrared (NIR) regions of the spectrum were studied. The relationships of canopy spectral reflectance or first derivative spectral reflectance with powdery mildew did not differ under different nitrogen input levels. However, the dynamics of VIs differed in their sensitivities to nitrogen input levels, disease severity, grain yield. The area of the red edge peak ( $\Sigma dr_{680-760\text{ nm}}$ ) was a better overall predictor for both disease severity and grain yield through linear regression models. The slope parameter estimates did not differ between the two nitrogen input levels at each GSs. Hyperspectral indices can be used to monitor wheat powdery mildew and estimate grain yield under different nitrogen input levels, but such models are dependent on GS and year, further research is needed to consider how to incorporate the growth stage and year-to-year variation into future applications.

**Keywords:** canopy hyperspectral reflectance; wheat powdery mildew; nitrogen input levels; detection models



**Citation:** Liu, W.; Sun, C.; Zhao, Y.; Xu, F.; Song, Y.; Fan, J.; Zhou, Y.; Xu, X. Monitoring of Wheat Powdery Mildew under Different Nitrogen Input Levels Using Hyperspectral Remote Sensing. *Remote Sens.* **2021**, *13*, 3753. <https://doi.org/10.3390/rs13183753>

Received: 22 August 2021

Accepted: 17 September 2021

Published: 18 September 2021

**Publisher's Note:** MDPI stays neutral with regard to jurisdictional claims in published maps and institutional affiliations.



**Copyright:** © 2021 by the authors. Licensee MDPI, Basel, Switzerland. This article is an open access article distributed under the terms and conditions of the Creative Commons Attribution (CC BY) license (<https://creativecommons.org/licenses/by/4.0/>).

## 1. Introduction

With the rapid development of remote sensing technology, hyperspectral remote sensing has recently become an important means of surface vegetation research. Remote sensing can be divided into near-ground remote sensing, aerial remote sensing, and satellite remote sensing according to the platform, of which near-ground remote sensing, including near-ground hyperspectral remote sensing, is the most studied in the monitoring of plant diseases [1–10].

Wheat powdery mildew, caused by the obligate fungi *Blumeria graminis* f. sp. *tritici* (*Bgt*), is one of the most important wheat diseases in the world [11,12]. Under greenhouse conditions, the reflectance within the ranges of 490–780 nm was the most sensitive to the powdery mildew severity [10]. Normalized difference vegetation index (NDVI) can also

be used to estimate wheat powdery mildew [13]. Most of the hyperspectral reflectance of healthy and mildewed wheat leaves in a laboratory was related to powdery mildew development [14]. A hyperspectral imager was used to identify mildew infected and healthy plant leaves [15]. Feng et al. [16] established a model relating wheat powdery mildew to the dual-green vegetation index. Previous studies also investigated using hyperspectral reflectance to detect wheat powdery mildew of several cultivars or at different planting densities [17,18]. These studies showed that the area of the red edge peak ( $\Sigma dr_{680-760 \text{ nm}}$ ), red edge slope ( $dr_{red}$ ), differential vegetation index (DVI), soil adjusted vegetation index (SAVI), triangular vegetation index (TVI), and several other spectral parameters were highly correlated with powdery mildew severity, of which  $\Sigma dr_{680-760 \text{ nm}}$  was the best. The intercepts often differed among varieties or planting densities, but the slopes did not.

Nitrogen fertilizers play a vital role in enhancing and stabilizing crop growth and yield [19]. Nitrogen application can cause changes in canopy reflectance [20–22]. Timely assessment of canopy nitrogen content is critical for precision crop management to ensure productivity as well as minimize adverse environmental impacts [23]. The canopy reflectance of wheat crops treated with different levels of nitrogen fertilizers decreased in both the visible region and the mid-infrared region but increased in the near-infrared region [24]. The whole-plant total N (between Feekes 3 and 6) could be used to predict N fertilizer requirements in winter wheat [25]. Due to the high correlation of absorption with chlorophyll (Chl) A, wheat N status could be estimated by the reflectance of wheat canopy at 550, 680 nm, the red edge position, and the reflectance ratio between 430 nm and 680 nm [26]. It was suggested that  $dr_{red}$  can be used as an indicator of winter wheat growth status, assisting in decision-making on fertilizers [27]. NDVI was a potentially useful vegetation index for wheat canopy nitrogen status [28]. However, hyperspectral reflectance of a canopy at different growth stages differed largely under varied N application rates but was consistent among different cultivars [29]. Both leaf nitrogen accumulation and canopy hyperspectral reflectance in wheat changed with N input levels, though consistent across cultivars and seasons [30]. N input levels varied significantly among farmers, and furthermore, large variability in N supply existed between and within fields [31,32]. These differences may potentially affect how the hyperspectral reflectance is to be used for monitoring mildew development.

Both the differences of nitrogen input levels and wheat powdery mildew severities can lead to changes in spectral reflectance. However, these two factors have been rarely studied simultaneously. To determine the effects and influences of different nitrogen input levels on monitoring wheat powdery mildew by near-ground hyperspectral remote sensing, the following studies were conducted: (1) Field trials were conducted for four consecutive seasons in 2016–2017, 2017–2018, 2018–2019, and 2019–2020 to study the use of the near-ground hyperspectral remote sensing technology to monitor wheat powdery mildew under different nitrogen input levels. (2) Then the obtained monitoring data were used to explore the impacts of different nitrogen input levels on mildew monitoring by the near-ground hyperspectral remote sensing.

## 2. Materials and Methods

**Plot design and yield determination.** Field experiments were conducted at the Langfang Experimental Station, Institute of Plant Protection, Chinese Academy of Agricultural Sciences (39.5°N, 116.6°E) in Hebei Province, China, in 2016–2017, 2017–2018, 2018–2019 and 2019–2020. Jingshuang 16, a winter wheat cultivar highly susceptible to powdery mildew, was sown in rows (inter-row distance of 0.25 m) with a seeding rate of 120 kg/ha on 7 October 2016, 2017, and 2018, and on 12 October 2019.

Two levels of nitrogen were used in all four seasons: standard regime (N1) and reduced input regime (N2). In 2016–2017 and 2017–2018, N1 consisted of the application before sowing: diammonium phosphate fertilizer (375 kg ha<sup>-1</sup>), urea (225 kg ha<sup>-1</sup>), potassium sulfate (150 kg ha<sup>-1</sup>); and a further application of urea (225 kg ha<sup>-1</sup>) in the early spring at growth stage (GS) 6 [33]. For N2, only 50% of the amount of fertilizers used in N1 were

used. In 2018–2019 and 2019–2020, the same amount of nitrogen was used for N1 as in the previous two seasons; but for N2, two-thirds of the amount of fertilizers used in N1 was used—thereafter named as N3. All treatments received the same input for both phosphorus and potassium fertilizers on the same dates as for nitrogen.

To create different levels of powdery mildew severities, there were six fungicide treatments [six concentrations of ethirimol (270, 240, 180, 120, 60, and 30 g active ingredient ha<sup>-1</sup>)] in addition to untreated control. Thus, in each season there were 14 treatments (seven fungicide treatments at each of the two levels of nitrogen input). A random block design (with three blocks) was used, giving a total of 42 plots, each plot was 5 m long and 4 m wide. Seedlings (sown in 10 cm pots) with sporulating *Bgt* lesions were maintained in a greenhouse compartment and transplanted to the center of each plot on 19 March 2017, 23 March 2018, 19 March 2019, and 14 March 2020 as spreaders to ensure powdery mildew development. The number of pots with *Bgt* spreaders corresponded to the concentrations of ethirimol for each plot: 6, 5, 4, 3, 2, 1, 0 pots plot<sup>-1</sup> for (0, 30, 60, 120, 180, 240, and 270 g active ingredient of ethirimol ha<sup>-1</sup>, respectively. This combination of ethirimol concentration and inoculum strength was used to create varying severities of powdery mildew. No other diseases and pests occurred in the field plots during the experimental periods.

Ethirimol was applied at an appropriate concentration on 15 April 2017, 15 April 2018, 17 April 2019, and 12 April 2020. The untreated control plots were sprayed with water. Manual weeding was carried out. At the harvest time, a subplot of 10 consecutive rows in each plot was randomly selected for harvesting. Rainy weather conditions in 2017 around GS 11.1 and 11.2 resulted in severe water lodging and, consequently, no grain yield data were available for the 2016–2017 growing season. Grains were threshed and dried under the sun before weighing.

Disease assessment. Powdery mildew was assessed at GS10.5.3, 10.5.4, and 11.1 in each year. Five positions in each plot (four at the corners and one at the center) were chosen for disease assessment; 20 plants at each position were assessed on a ‘0-to-9’ scale [34,35]. Disease index (DI) for a plot was estimated as:

$$DI = \sum_{i=0}^{i=9} i * n_i / 9 * \sum_{i=0}^{i=9} n_i \times 100 \quad (1)$$

where  $n_0, n_1, \dots, n_9$  are the number of plants with mildew severity values of 0, 1, . . . 9, respectively.

Reflectance measurement. Canopy percentage reflectance data were acquired with an ASD Field Spec Pro spectrometer (Analytical Spectral Devices, Boulder, CO, USA) at the same time when mildew was assessed. This spectrometer has a sampling interval of 1.4 nm in the region of 350 to 1050 nm (3 nm spectral resolution) and 2 nm in the 1050 to 2500 nm region (10-nm spectral resolution), with a field of view of 25°. Both 1.4 nm and 2 nm sampling intervals were automatically interpolated to 1 nm intervals by the instrument. The sensor, facing downwards at the center of the plot, was positioned 0.5 m from the top of the wheat canopy, covering a 22.16 cm diameter field of view. Measurements were taken on clear, sunny days between 10:00 h and 14:00 h (Beijing time, GMT + 8:00). The instrument was referenced to a calibrated spectral on a white reflectance panel about every 15 min, allowing readings from different assessment dates to be compared. On each sampling date, 20 different positions near the center were used and the average value was used for further analysis.

Data analysis. Through Viewspec Program software (ASD Company), the original reflectance spectrum data of canopy, reflectance spectrum data, the reflectance curve, and first derivative spectra were obtained. To identify indices for assessing wheat powdery mildew severity, smoothed raw reflectance data were combined into nine spectral indices (SIs), including two red edge parameters from the first derivative reflectance, three derived from reflectance of broad-band, and four from reflectance of single-band (Table 1). Among the nine indices, red edge slope ( $d_{\lambda red}$ ), the area of the red edge peak ( $\Sigma_{dr680-760 nm}$ ), difference vegetation index (DVI), normalized difference vegetation index (NDVI), and

triangular vegetation index (TVI) were useful for wheat powdery mildew monitoring under certain conditions, whilst green normalized difference vegetation index (GNDVI), nitrogen reflectance index (NRI), the transformed chlorophyll absorption and reflectance index (TCARI), modified chlorophyll absorption ratio index (MCARI) were all related to the Chl concentration as well as N concentrations. On the other hand, there were significant differences in spectral reflectance indices of wheat at different GSs. Photochemical reflectance index (PRI), which was widely used for estimation of plant stress changes, was also analyzed, but the results were not shown because of its poor correlations with disease severity and yield.

**Table 1.** Vegetation indices used in this study and their calculation.

Spectral Indices	Description or Formula	Literatures
Reflectance of green band ( $R_{Green}$ )	Reflectance of green band within 560–600 nm	
Reflectance of red band ( $R_{Red}$ )	Reflectance of red band within 650–680 nm	
Reflectance of near-infrared band ( $R_{NIR}$ )	Reflectance of near-infrared band within 780–890 nm	
Red edge slope ( $d_{\lambda red}$ )	Maximum value of 1st derivative within the red edge	[36]
The area of the red edge peak ( $\Sigma dr_{680-760 nm}$ )	The area under the 1st derivative curve in the red edge region	[36]
Difference vegetation index (DVI)	$R_{NIR} - R_{Red}$	[37]
Normalized difference vegetation index (NDVI)	$(R_{NIR} - R_{Red}) / (R_{NIR} + R_{Red})$	[38]
Green normalized difference vegetation index (GNDVI)	$(R_{NIR} - R_{Green}) / (R_{NIR} + R_{Green})$	[39]
Nitrogen reflectance index (NRI)	$(R_{570 nm} - R_{670 nm}) / (R_{570 nm} + R_{670 nm})$	[26]
Triangular vegetation index (TVI)	$0.5[120(R_{750 nm} - R_{550 nm}) - 200(R_{670 nm} - R_{550 nm})]$	[40]
The transformed chlorophyll absorption and reflectance index (TCARI)	$3[(R_{700 nm} - R_{670 nm}) - 0.2(R_{700 nm} - R_{550 nm})(R_{700 nm} / R_{670 nm})]$	[41]
Modified chlorophyll absorption ratio index (MCARI)	$(R_{701 nm} - R_{671 nm}) - 0.2(R_{701 nm} - R_{549 nm}) / (R_{701 nm} / R_{671 nm})$	[42]

Initial correlation analysis suggested that canopy reflectance  $\Sigma dr_{680-760 nm}$  is the best overall predictor of wheat powdery mildew severity and grain yield. Thus, linear regression of mildew DI and yield with  $\Sigma dr_{680-760 nm}$  was carried (SAS Institute Inc., Cary, NC, USA). Initially, linear regression modeling was used to estimate the variability in the mildew disease index or grain yield accounted for by nitrogen input levels, growth stages,  $\Sigma dr_{680-760 nm}$ , and their interactions; in this analysis, the season was treated as a blocking factor. This initial analysis suggested large effects of season and growth stage on the mildew DI/yield –  $\Sigma dr_{680-760 nm}$  relationships. Thus, regression analysis was applied to each combination of season and growth stage for testing the effects of nitrogen input on mildew DI/yield –  $\Sigma dr_{680-760 nm}$  relationships through parallel curve analysis.

### 3. Results

#### 3.1. Relationships between Powdery Mildew and Canopy Spectral Reflectance of Wheat

The overall patterns of correlation of canopy spectral reflectance with mildew DI were similar at the three growth stages under both the standard and reduced nitrogen input levels in all four seasons (Figure 1). Correlation between the spectral reflectance in the visible red wavelengths (650–680 nm) and DI differed in its magnitude among seasons; for the low nitrogen input treatment, the correlation was only significant at GS10.5.3 in 2017, and GS11.1 in 2019 and 2020. There was no significant correlation between the reflectance of the red band and DI for the standard nitrogen input treatment. The reflectance of the near-infrared band (750–880 nm) was negatively correlated with DI: the correlation coefficient was less than  $-0.50$ .

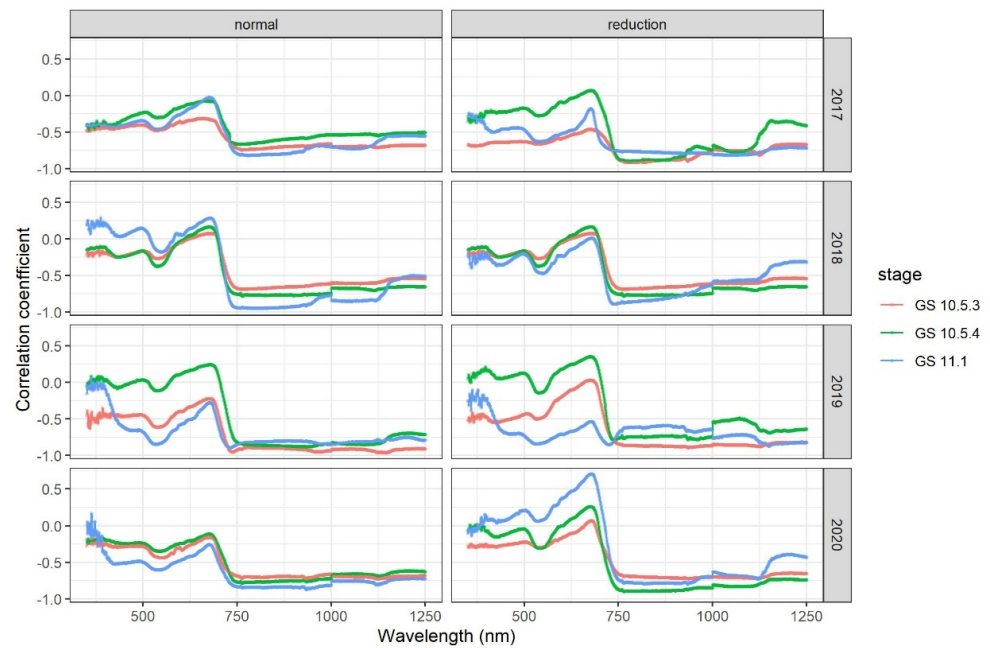


**Figure 1.** Correlation coefficient of wheat powdery mildew index (DI) with spectral reflectance of wheat canopy at GS10.5.3, GS10.5.4 and GS11.1 under two nitrogen input levels (standard and reduced) in 2017–2020.

### 3.2. Relationships between Disease Index and the First Derivative Spectrum

The correlation of DI with the first derivative spectrum of canopy reflectance was similar except for small differences between the two nitrogen input levels (Figure 2). Correlation varied greatly at 353–500 nm among three growth stages, but was consistently large and negative (often  $< -0.5$ ) at 500–550 nm. Most of the correlations at the green (560–600 nm) and red band (650–670 nm) were large and positive, whereas most of the correlations at the red-edge band (680–760 nm) were large and negative.

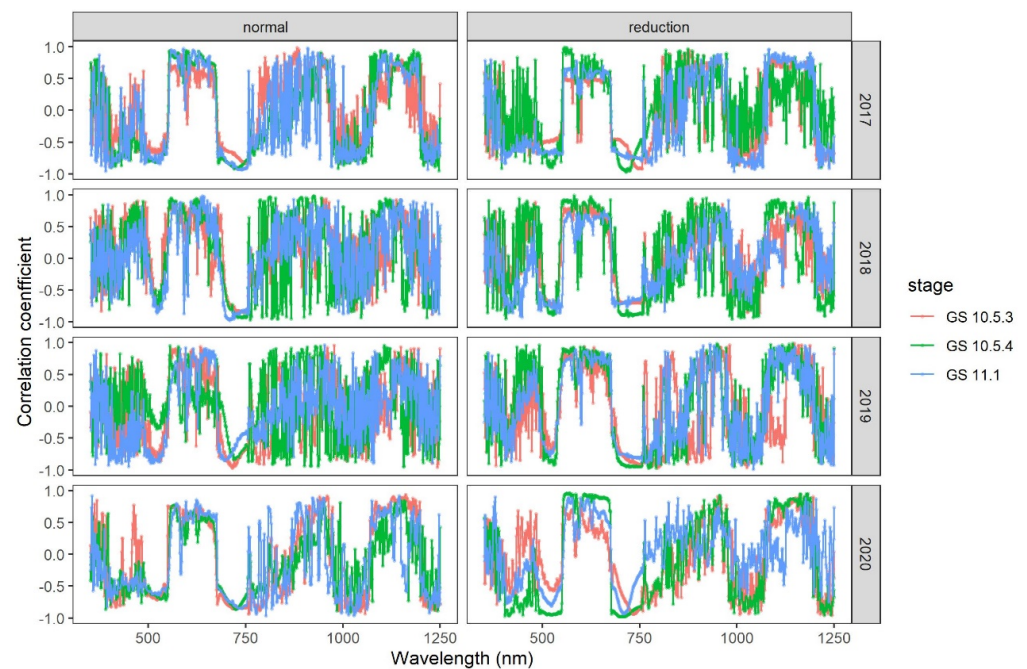


**Figure 2.** Correlation between the first derivative spectrum and wheat powdery mildew index (DI) at GS10.5.3, GS10.5.4 and GS11.1 stage under the two nitrogen input levels in 2017–2020.

### 3.3. Correlation between Disease Index and Spectral Parameters

Figure 3 shows the correlation of mildew DI with spectral parameter variables.  $dr_{red}$ ,  $\Sigma dr_{680-760\text{ nm}}$ , DVI, NRI, and TVI were significantly correlated negatively with DI under both nitrogen input levels at all three growth stages in the four seasons. Correlation coefficients ranged from  $-0.87$  to  $-0.41$ ,  $-0.89$  to  $-0.45$ ,  $-0.89$  to  $-0.48$ ,  $-0.78$  to  $-0.44$ , and  $-0.90$  to  $-0.50$  for  $dr_{red}$ ,  $\Sigma dr_{680-760\text{ nm}}$ , DVI, NRI, and TVI, respectively. Most of the correlation of DI with NDVI, GNDVI, TCARI, and MCARI was significant and negative, ranging from  $-0.74$  to  $-0.10$ ,  $-0.68$  to  $-0.01$ ,  $-0.89$  to  $-0.31$ , and  $-0.79$  to  $-0.26$ , respectively.

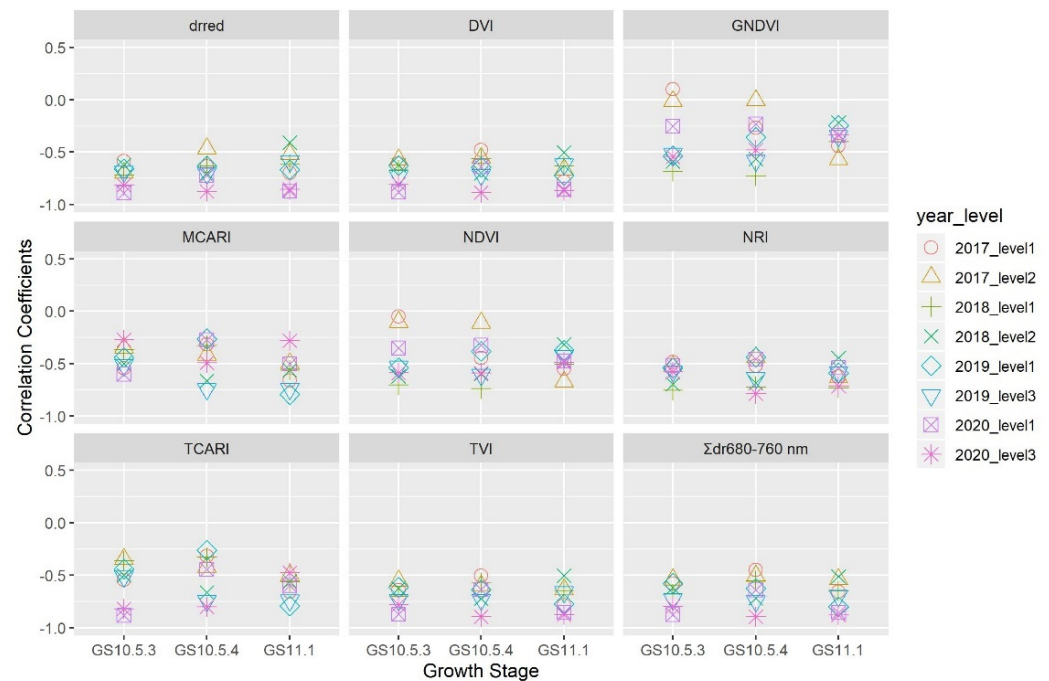


**Figure 3.** Correlation coefficients of wheat powdery mildew index with spectral parameters under different nitrogen input levels at three growth stages over four seasons; ‘○’, ‘△’, ‘+’, ‘×’, ‘◇’, ‘▽’, ‘□’, ‘\*’ represent the year-level combinations 2017–level1, 2017–level2, 2018–level1, 2018–level2, 2019–level1, 2019–level3, 2020–level1 and 2020–level3, respectively.

### 3.4. Relationships between Disease Index and Canopy Spectral Reflectance

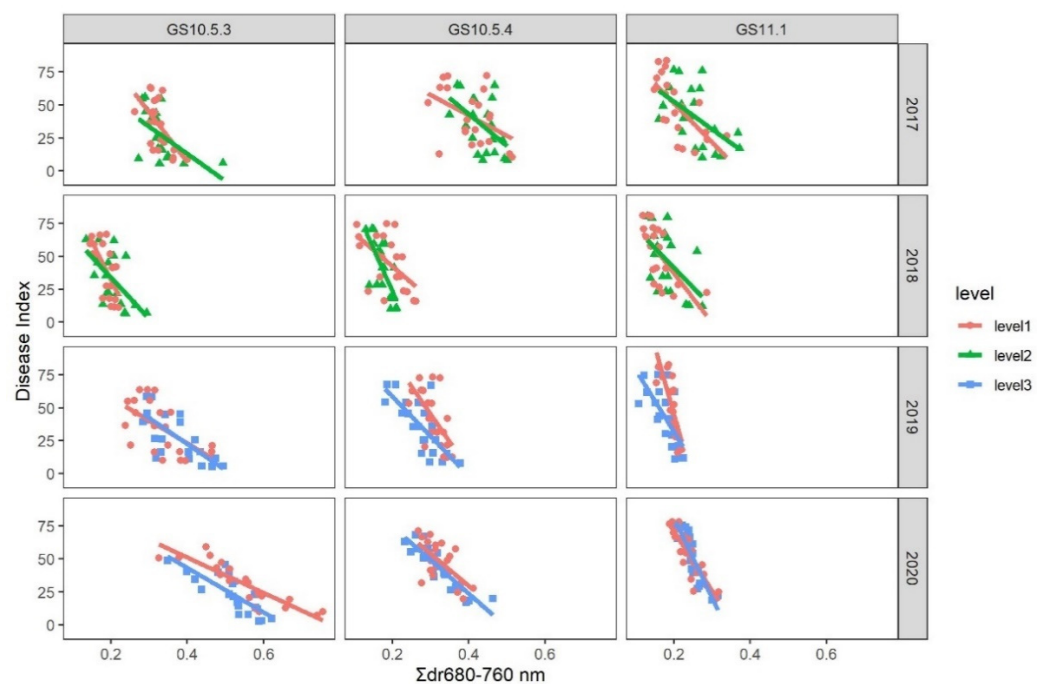
$\Sigma dr_{680-760\text{ nm}}$  was consistently correlated highly with DI and thus used in linear regression. Table 2 shows the overall contribution of experimental factors to the observed variation in wheat mildew DI. The effect of year, nitrogen input, and growth stage (i.e., on the intercept) were significant, accounting for 8.5%, 1.8%, and 1.0% of the total variability, respectively. The interaction between  $\Sigma dr_{680-760\text{ nm}}$  and growth stage was significant ( $p < 0.001$ ), suggesting the slope parameter in the DI-  $\Sigma dr_{680-760\text{ nm}}$  relationship varied with the growth stage. However, the residual error was still large, accounting for 57.2% of the variability in DI, including variation due to possible interaction of season with other variables.

**Table 2.** ANOVA summary of linear regression of wheat powdery mildew index (DI) on nitrogen input levels, growth stages and  $\Sigma dr_{680-760\text{ nm}}$  (a spectral parameter derived from canopy reflectance).

Parameter	Df	Sum Sq	Mean Sq	F Value	Pr (>F)
$\Sigma dr_{680-760\text{ nm}}$	1	44,753	44,753	172.47	$2 \times 10^{-16}$ ***
Year	3	18,520	6173	23.79	$2.24 \times 10^{-14}$ ***
Nitrogen input level	2	3906	1953	7.53	0.00061 ***
Growth stage	2	2237	1119	4.31	0.0139 *
$\Sigma dr_{680-760\text{ nm}}$ * nitrogen input level	2	75	38	0.14	0.865
$\Sigma dr_{680-760\text{ nm}}$ * growth stage	2	12,941	6471	24.94	$4.94 \times 10^{-11}$ ***
Nitrogen input level * growth stage	4	6521	1630	6.28	$6.20 \times 10^{-5}$ ***
$\Sigma dr_{680-760\text{ nm}}$ * nitrogen input level * growth stage	4	4713	1178	4.54	0.00131 **
Residuals	483	125,332	259		
Total	503	218,998	435		

Signif. codes: 0 '\*\*\*' 0.001 '\*\*' 0.01 '\*' 0.05.

Because of the significant interaction between growth stage and  $\Sigma dr_{680-760\text{ nm}}$  as well as considerable among-season variability, we fitted regression models of DI with  $\Sigma dr_{680-760\text{ nm}}$  for each combination of growth stage and season (Figure 4). Parallel curve analysis showed that there was no significant difference in the slope between the two nitrogen input levels at every GS in each season. There was no significant difference in the intercept between the two nitrogen input levels except in GS10.5.4, GS11.1 in the 2018–2019 season, and GS10.5.3 in the 2019–2020 season (Table 3).

**Figure 4.** Fitted regression models relating  $\Sigma dr_{680-760\text{ nm}}$  (a spectral parameter derived from canopy reflectance) to powdery mildew index on winter wheat at two nitrogen input levels among different growth stages and years.

**Table 3.** Linear regression of wheat powdery mildew index (DI) on  $\Sigma dr_{680-760\text{ nm}}$  at the two nitrogen input levels at different growth stages in four seasons. Parallel curve analysis was conducted to assess the effect of nitrogen input on the intercept and slope estimates.

Season	Growth Stage	Level 1	Level 2	Parallel Curve Analysis
2016–2017	10.5.3	$y = -376.6x + 157.5$	$y = -206.4x + 95.6$	F = 0.45, $p = 0.716$ for slope; F = 1.14, $p = 0.347$ for intercept
	10.5.4	$y = -155.2x + 104.2$	$y = -241.9x + 140.0$	F = 0.60, $p = 0.617$ for slope; F = 1.73, $p = 0.179$ for intercept
	11.1	$y = -296.3x + 110.6$	$y = -210.1x + 94.7$	F = 0.34, $p = 0.795$ for slope; F = 2.15, $p = 0.113$ for intercept
2017–2018	10.5.3	$y = -578.8x + 147.8$	$y = -312.0x + 96.3$	F = 0.52, $p = 0.673$ for slope; F = 0.47, $p = 0.702$ for intercept
	10.5.4	$y = -249.3x + 92.4$	$y = -651.6x + 153.7$	F = 0.35, $p = 0.790$ for slope; F = 1.22, $p = 0.317$ for intercept
	11.1	$y = -374.7x + 112.1$	$y = -299.2x + 101.3$	F = 0.16, $p = 0.923$ for slope; F = 0.88, $p = 0.459$ for intercept
2018–2019	10.5.3	$y = -172.7x + 92.0$	$y = -198.0x + 101.6$	F = 1.20, $p = 0.325$ for slope; F = 1.86, $p = 0.156$ for intercept
	10.5.4	$y = -421.0x + 171.3$	$y = -301.5x + 118.8$	F = 1.23, $p = 0.315$ for slope; F = 5.77, $p = 0.0027$ for intercept
	11.1	$y = -1026.6x + 250.1$	$y = -468.8x + 125.5$	F = 0.90, $p = 0.452$ for slope; F = 5.06, $p = 0.0052$ for intercept
2019–2020	10.5.3	$y = -134.3x + 104.8$	$y = -168.9x + 110.8$	F = 1.38, $p = 0.266$ for slope; F = 6.06, $p = 0.002$ for intercept
	10.5.4	$y = -245.3x + 127.6$	$y = -254.9x + 125.6$	F = 2.19, $p = 0.108$ for slope; F = 1.54, $p = 0.223$ for intercept
	11.1	$y = -451.1x + 161.3$	$y = -608.1x + 202.8$	F = 1.45, $p = 0.244$ for slope; F = 1.25, $p = 0.307$ for intercept

The *df* of Parallel curve analysis at every GS in each season was 20.

### 3.5. Correlation between Wheat Yield and Spectral Parameters

Correlations between grain yield and spectral parameter variables are given in Table 4. Grain yield was positively correlated with  $dr_{red}$ ,  $\Sigma dr_{680-760\text{ nm}}$ , DVI, NRI, TVI, NDVI, GNDVI, TCARI, and MCARI, but there were differences in these correlation coefficients among different nitrogen input levels and growth stages. Of which  $dr_{red}$ ,  $\Sigma dr_{680-760\text{ nm}}$ , DVI, NRI, and TVI were significantly positively with grain yield, in contrast, correlation of grain yield with NDVI, GNDVI, TCARI, and MCARI was inconsistent.

### 3.6. Relationships of Grain Yield with Spectral Parameter Variables

Because of its consistent correlation with grain yield,  $\Sigma dr_{680-760\text{ nm}}$  was used in linear regression. Table 5 shows the overall contribution of experimental factors to the observed variation in grain yield. The effects of year, nitrogen input, and growth stage were all significant (differing intercept) and accounted for 20.1%, 10.5%, and 3.4% of the total variability, respectively. The interaction between  $\Sigma dr_{680-760\text{ nm}}$  and nitrogen input level or growth stage both were significant ( $p < 0.001$ ), suggesting the slope parameter in the yield- $\Sigma dr_{680-760\text{ nm}}$  relationship varied with nitrogen input level and growth stage. However, the residual error accounted for 20% of the variability in yield.

**Table 4.** Coefficients of correlation between spectral parameters under different nitrogen input levels at three growth stages over three seasons and grain yield.

Year	Parameter	Level 1			Level 2		
		GS10.5.3	GS10.5.4	GS11.1	GS10.5.3	GS10.5.4	GS11.1
2018	$dr_{red}$	0.71 **	0.68 **	0.63 **	0.54 *	0.64 **	0.38
	$\Sigma dr_{680-760\text{ nm}}$	0.65 **	0.60 **	0.65 **	0.51 *	0.63 **	0.46 *
	DVI	0.77 **	0.79 **	0.60 **	0.52 *	0.58 *	0.32
	NDVI	0.73 **	0.75 **	0.58 **	0.54 *	0.51 *	0.28
	GNDVI	0.71 **	0.73 **	0.47 *	0.52 *	0.60 **	0.2
	NRI	0.79 **	0.77 **	0.79 **	0.62 **	0.65 **	0.39
	TVI	0.68 **	0.62 **	0.66 **	0.52 *	0.64 **	0.46 *
	TCARI	0.3	0.38	0.54 *	0.37	0.56 **	0.50 *
	MCARI	0.31	0.38	0.54 *	0.37	0.56 **	0.50 *
2019	$dr_{red}$	0.70 **	0.63 **	0.69 **	0.74 **	0.70 **	0.66 **
	$\Sigma dr_{680-760\text{ nm}}$	0.60 **	0.64 **	0.82 **	0.76 **	0.74 **	0.76 **
	DVI	0.62 **	0.42	0.36	0.60 **	0.55 **	0.45 *
	NDVI	0.60 **	0.36	0.4	0.57 **	0.54 *	0.51 *
	GNDVI	0.59 **	0.32	0.27	0.56 **	0.52 *	0.43
	NRI	0.63 **	0.43	0.61 **	0.61 **	0.59 **	0.66 **
	TVI	0.65 **	0.65 **	0.80 **	0.77 **	0.73 **	0.73 **
	TCARI	0.46 *	0.31	0.79 **	0.50 *	0.75 **	0.75 **
	MCARI	0.45 *	0.31	0.80 **	0.50 *	0.75 **	0.75 **
2020	$dr_{red}$	0.83 **	0.87 **	0.88 **	0.90 **	0.83 **	0.72 **
	$\Sigma dr_{680-760\text{ nm}}$	0.82 **	0.84 **	0.90 **	0.88 **	0.84 **	0.77 **
	DVI	0.82 **	0.84 **	0.90 **	0.89 **	0.85 **	0.76 **
	NDVI	0.4	0.26	0.42	0.59 **	0.60 **	0.37
	GNDVI	0.31	0.15	0.31	0.56 **	0.52 *	0.23
	NRI	0.54 *	0.44 *	0.44 *	0.55 **	0.72 **	0.62 **
	TVI	0.81 **	0.84 **	0.89 **	0.86 **	0.84 **	0.77 **
	TCARI	0.84 **	0.64 **	0.63 **	0.87 **	0.72 **	0.47 *
	MCARI	0.49 *	0.46 *	0.56 **	0.36	0.43	0.31

Significance levels for the correlation coefficients:  $0.01 < p \leq 0.05$  (\*),  $p \leq 0.01$  (\*\*).

**Table 5.** ANOVA summary of linear regression of grain yield on nitrogen input levels, growth stages and  $\Sigma dr_{680-760\text{ nm}}$  (a spectral parameter derived from canopy reflectance).

Parameter	Df	Sum Sq	Mean Sq	F Value	Pr (>F)
$\Sigma dr_{680-760\text{ nm}}$	1	59.63	59.63	668.89	$<2.2 \times 10^{-16}$ ***
Year	2	32.11	16.06	180.10	$<2.2 \times 10^{-16}$ ***
Nitrogen input level	2	16.77	8.38	94.04	$<2.2 \times 10^{-16}$ ***
Growth stage	2	5.37	2.68	30.10	$8.26 \times 10^{-13}$ ***
$\Sigma dr_{680-760\text{ nm}}$ * nitrogen input level	2	1.36	0.68	7.62	0.000573 ***
$\Sigma dr_{680-760\text{ nm}}$ * growth stage	2	8.61	4.30	48.28	$<2.2 \times 10^{-16}$ ***
Nitrogen input level * growth stage	4	2.11	0.53	5.93	0.000126 ***
$\Sigma dr_{680-760\text{ nm}}$ * nitrogen input level * growth stage	4	1.55	0.39	4.34	0.00194 **
Residuals	358	31.91	0.089		
Total	377	159.47	0.42		

Signif. codes: 0 '\*\*\*' 0.001 '\*\*' 0.01 '\*' 0.05.

Because of the significant interaction between  $\Sigma dr_{680-760\text{ nm}}$  and nitrogen input level or growth stage as well as considerable among-season variability, models relating grain yield to  $\Sigma dr_{680-760\text{ nm}}$  were fitted to an individual combination of growth stage and season (Figure 5). Parallel curve analysis showed that there was no significant difference in the slope at every GS between the two nitrogen input levels in each season; however, there was a significant difference in the intercept between the two nitrogen input levels in GS10.5.3,

GS11.1 in 2017–2018 season, GS10.5.3 in the 2018–2019 season, and GS11.1 in the 2019–2020 season (Table 6).

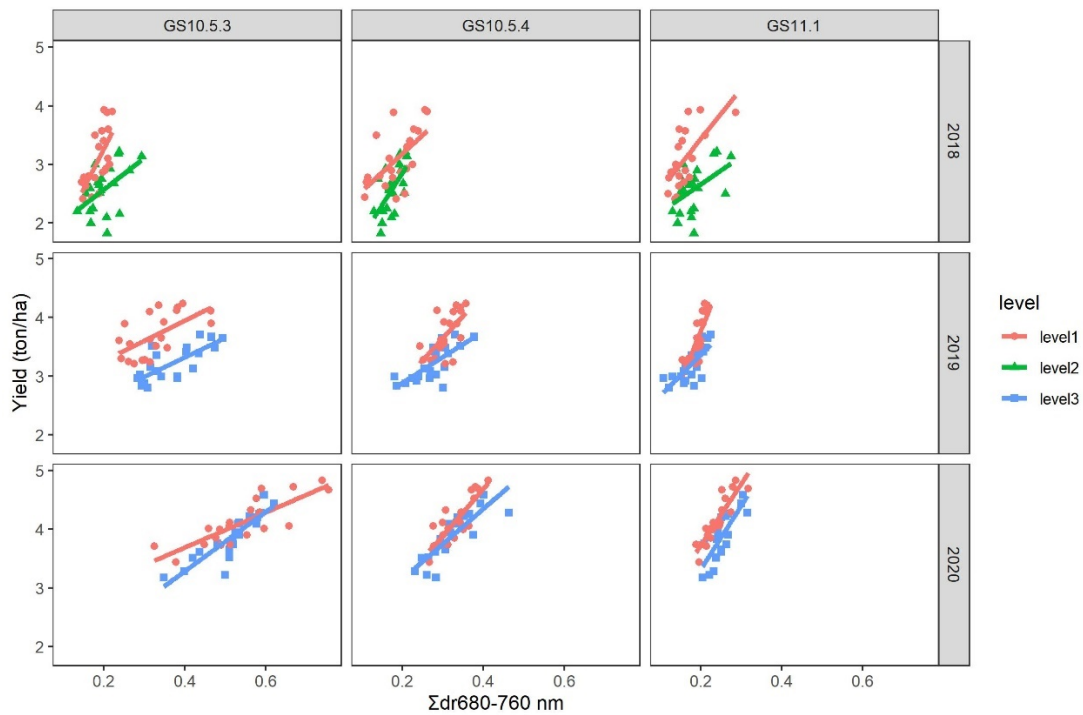


**Figure 5.** Fitted regression models relating  $\Sigma dr_{680-760\text{ nm}}$  (a spectral parameter derived from canopy reflectance) to grain yield at two nitrogen input levels among different growth stages and years.

**Table 6.** Linear regression of grain yield on  $\Sigma dr_{680-760\text{ nm}}$  at the two nitrogen input levels at different growth stages in three seasons. Parallel curve analysis was conducted to assess the effect of nitrogen input on the intercept and slope estimates.

Season	Growth Stage	Level 1	Level 2	Parallel Curve Analysis
2017–2018	10.5.3	$y = 13.63x + 0.54$	$y = 5.36x + 1.50$	F = 0.59, $p = 0.627$ for slope; F = 3.74, $p = 0.020$ for intercept
	10.5.4	$y = 6.37x + 1.91$	$y = 10.91x + 0.68$	F = 0.36, $p = 0.780$ for slope; F = 0.68, $p = 0.569$ for intercept
	11.1	$y = 8.60x + 0.72$	$y = 4.74x + 1.71$	F = 0.39, $p = 0.761$ for slope; F = 4.92, $p = 0.0061$ for intercept
2018–2019	10.5.3	$y = 3.44x + 2.57$	$y = 3.31x + 2.0$	F = 1.81, $p = 0.164$ for slope; F = 11.56, $p < 0.001$ for intercept
	10.5.4	$y = 7.56x + 1.38$	$y = 4.42x + 2.0$	F = 1.76, $p = 0.173$ for slope; F = 0.21, $p = 0.888$ for intercept
	11.1	$y = 17.01x + 0.37$	$y = 6.98x + 1.97$	F = 2.34, $p = 0.0911$ for slope; F = 0.74, $p = 0.536$ for intercept
2019–2020	10.5.3	$y = 2.99x + 2.49$	$y = 5.06x + 1.26$	F = 1.09, $p = 0.366$ for slope; F = 0.45, $p = 0.722$ for intercept
	10.5.4	$y = 7.95x + 1.50$	$y = 5.99x + 1.95$	F = 0.79, $p = 0.508$ for slope; F = 2.35, $p = 0.0895$ for intercept
	11.1	$y = 10.50x + 1.62$	$y = 10.87x + 1.14$	F = 2.5, $p = 0.0764$ for slope; F = 11.33, $p < 0.001$ for intercept

The *df* of Parallel curve analysis at every GS in each season was 20.

#### 4. Discussion

Canopy hyperspectral reflectance data were acquired at Feekes growth stage (GS) 10.5.3, 10.5.4, and 11.1 under different nitrogen input levels in four consecutive seasons. The trend of the relationships between canopy spectral reflectance and wheat powdery mildew was basically consistent under different nitrogen input levels, especially the reflectance in the near-infrared band (750–880 nm) was significantly correlated negatively with wheat powdery mildew. Cao et al. [17,18] also found that there was a significant negative correlation between spectral reflectance in the near-infrared band and disease index of wheat powdery mildew. On the other hand, different N rates markedly influenced the characteristics of spectral reflectance of the wheat canopy, with different spectral responses in near-infrared regions [30], these results indicated that it was feasible to monitor wheat powdery mildew with near-infrared reflectance under different nitrogen input levels. The first derivative processing can reduce the low frequency background noise and improve the overlapping spectral resolution [43], in this study, it was found that the disease index of wheat powdery mildew was significantly correlated with the first derivative spectrum of most green light bands, red light bands, and red edge bands, this indicated that the occurrence of wheat powdery mildew can be monitored by using the first derivative spectrum of visible light band. Malthus and Madeira [44] also found that the first derivative spectrum of the visible light band can be used to monitor field bean leaves infected by *botrytis fabae*.

Most spectral variables derived from the canopy hyperspectral reflectance data were highly correlated to the disease index of wheat powdery mildew and grain yield under different nitrogen input levels, the mathematical calculation methods of these variables may relate to the variation in performance of the vegetative indices in disease detection. For  $dr_{red}$  and  $\Sigma dr_{680-760\text{ nm}}$  were significantly correlated with disease index of wheat powdery mildew at GS10.5.3, 10.5.4, and 11.1 in the four/three seasons under the two nitrogen input levels, this can be explained by the fact that  $\Sigma dr_{680-760\text{ nm}}$  is calculated from wavelengths between 680 and 760 nm and most of the correlations between the first derivative spectrum at 680–760 nm and disease index of wheat powdery mildew were significant (Figure 2). The  $dr_{red}$  was less correlated with disease index than  $\Sigma dr_{680-760\text{ nm}}$  this was because  $dr_{red}$  on the rate of reflectance increases between visible and near-infrared. For SIs calculated based on the combination of reflectance of broad-band, especially includes NIR wavebands, DVI had more significant correlations with disease index than NDVI and GNDVI in all seasons under the two nitrogen input levels, indicating that DVI was more appropriate for disease detection, this was accordant with its mathematical calculation methods of DVI which has been shown to have a low error with dense canopies [40]. TVI, calculated from the differences in reflectance of 550 nm, 670 nm, and 750 nm wavelengths, had a significant correlation with disease index and grain yield, three typical peak inflection points exist near 550 nm, 670 nm, and 750 nm bands in every nitrogen input level and growth stage. The performance of NRI was consistently correlated with disease index and grain yield during the four/three growing seasons, indicating that NRI is able to detect wheat powdery mildew under different nitrogen input levels.

The parallel curve analysis of disease/yield- $\Sigma dr_{680-760\text{ nm}}$  models within individual seasons at a single growth stage showed that there were no significant differences in the slope among nitrogen input levels, but some significant differences in the intercept of the models, indicated that there were differences between canopy reflectance at different nitrogen input levels, which is consistent with previous studies [45,46], and existing studies have suggested that varied N management practices result in differences in leaf area index, biomass, leaf chlorophyll, and tissue N concentrations that in turn contribute to the differences in canopy spectral reflectance [24]. However, when analyzed over all the four/three season, suggested that both the intercept and slope estimates in the DI/yield- $\Sigma dr_{680-760\text{ nm}}$  relationship could be affected greatly by growth stage and/or nitrogen input, particularly wheat yield. These differences are primarily due to the fact that growth stage and year effects were implicitly incorporated into the models when models were fitted to individual seasons at a single growth stage.

Although remote sensing is a potential alternative for detecting wheat powdery mildew, rather than a visual assessment of plants, further work is necessary before the method can be adopted for practical use, such as the influence of some other factors on spectral monitoring or relational model of wheat powdery mildew needs to be clarified. Our study found that there existed certain differences in the intercepts of wheat powdery mildew monitoring models by canopy hyperspectral reflectance under different nitrogen input levels and growth stages, moreover, studies also had found that there were some differences in the detecting models under different wheat varieties [17] and different planting densities [18], these results indicated that the wheat variety, planting density, growth stage and nitrogen input level could cause differences in hyperspectral reflectance monitoring models of wheat powdery mildew, and such differences would greatly limit the application of hyperspectral reflectance in monitoring wheat powdery mildew in the field.

The exact relationship of lgR (remote imaging parameter) with disease severity and grain yield varied considerably from year to year, which raised an important question about the consistency of using remote imaging information to estimate disease severity and grain yield [47]. In the present study, the main season effect accounted for 8.5% and 20.1% of the variability in mildew DI or yield, respectively; hence the intercept estimate varied significantly between seasons. In addition, there still existed large residuals in powdery mildew or grain yield regression models, accounting for 57.2% and 20% of the respective variability in DI and or yield. This large residual variation may also include the possible interaction of the season with other variables. The present study thus suggested that the relationship can be used to estimate relative disease severity and yield within a given year and growth stage and that these models still could be useful if we have information about the initial level of disease to adjust the relative disease level into an absolute level, although it is much difficult to estimate the absolute level of disease severity. The large seasonal effect on the observed relationships of mildew severity/yield with canopy reflectance raises an important issue, namely, how to develop and/or apply a common model to different seasons without losing many predictive accuracies. Further research is needed to consider how to incorporate the year-to-year and growth stage effects into future applications.

## 5. Conclusions

This study demonstrated that canopy hyperspectral reflectance can be used in wheat powdery mildew detection and estimate grain yield under different nitrogen input levels. However, the dynamics of VIs differed in their sensitivities to nitrogen input levels, disease severity and grain yield. The area of the red edge peak ( $\sum dr_{680-760\text{ nm}}$ ) was a better overall predictor for both disease severity, and grain yield through linear regression models. The slope parameter estimates did not differ between the two nitrogen input levels at each GSs, but some significant differences in the intercept indicated that there were differences between canopy reflectance at different nitrogen input levels, mainly due to the growth stage and year-to-year variation. Further research is needed to consider how to incorporate the year-to-year and growth stage effects into future applications.

**Author Contributions:** Conceived and designed the experiments: W.L., J.F., X.X., Y.Z. (Yilin Zhou), Performed the experiments: W.L., C.S., Y.Z. (Yanan Zhao), F.X., J.F., Analyzed the data: W.L., F.X., Y.S., X.X., Y.Z. (Yilin Zhou), Contributed reagents/materials/analysis tools: W.L., Y.S., X.X., Y.Z. (Yilin Zhou), Wrote the paper: W.L., C.S., Y.Z. (Yanan Zhao), F.X., X.X., J.F., Y.Z. (Yilin Zhou). All authors have read and agreed to the published version of the manuscript.

**Funding:** This work was financially supported by the National Natural Science Foundation of China (31901826), National Key Research and Development Program of China (2017YFD0201700), and UK Science Technology Facilities Council (project number: ST/V00137X/1).

**Institutional Review Board Statement:** Not applicable.

**Informed Consent Statement:** Not applicable.

**Conflicts of Interest:** The authors declare no conflict of interest.

## References

1. Ausmus, B.S.; Hilty, J.W. Reflectance studies of healthy, maize dwarf mosaic virus-infected, and *Helminthosporium maydis*-infected corn leaves. *Remote Sens. Environ.* **1972**, *2*, 77–81. [[CrossRef](#)]
2. Zhang, M.; Qin, Z. Detection of stress in tomatoes induced by late blight disease in California, USA, using hyperspectral remote sensing. *Int. J. Appl. Earth Obs* **2003**, *4*, 295–310. [[CrossRef](#)]
3. Ashourloo, D.; Mobasheri, M. Developing two spectral disease indices for detection of wheat leaf rust (*Puccinia triticina*). *Remote Sens.* **2014**, *6*, 4723–4740. [[CrossRef](#)]
4. Ashourloo, D.; Mobasheri, M. Evaluating the effect of different wheat rust disease symptoms on vegetation indices using hyperspectral measurements. *Remote Sens.* **2014**, *6*, 5107–5123. [[CrossRef](#)]
5. Mahlein, A.K.; Steiner, U. Spectral signatures of sugar beet leaves for the detection and differentiation of diseases. *Precis. Agric.* **2010**, *11*, 413–431. [[CrossRef](#)]
6. Muhammed, H.H.; Larsolle, A. Feature vector based analysis of hyperspectral crop reflectance data for discrimination and quantification of fungal disease severity in wheat. *Biosyst. Eng.* **2003**, *86*, 125–134. [[CrossRef](#)]
7. Yang, C.M. Assessment of the severity of bacterial leaf blight in rice using canopy hyperspectral reflectance. *Precis. Agric.* **2010**, *11*, 61–81. [[CrossRef](#)]
8. Bauriegel, E.; Giebel, A. Early detection of Fusarium infection in wheat using hyper-spectral imaging. *Comput. Electron. Agric.* **2011**, *75*, 304–312. [[CrossRef](#)]
9. Chen, B.; Li, S.K. Evaluating the severity level of cotton verticillium using spectral signature analysis. *Int. J. Remote Sens.* **2012**, *33*, 2706–2724. [[CrossRef](#)]
10. Graeff, S.; Link, J. Identification of powdery mildew (*Erysiphe graminis* f. sp. *tritici*) and take-all disease (*Gaeumannomyces graminis* sp. *tritici*) in wheat (*Triticum aestivum* L.) by means of leaf reflectance measurements. *Cent. Eur. J. Biol.* **2006**, *1*, 275–288.
11. Bennett, F.G.A. Resistance to powdery mildew in wheat: A review of its use in agriculture and breeding programmes. *Plant Pathol.* **1984**, *33*, 279–300. [[CrossRef](#)]
12. Cao, X.R.; Yao, D.M. Development of weather- and airborne inoculum-based models to describe disease severity of wheat powdery mildew. *Plant Dis.* **2015**, *99*, 395–400. [[CrossRef](#)]
13. Franke, J.; Menz, G. Multi-temporal wheat disease detection by multi-spectral remote sensing. *Precis. Agric.* **2007**, *8*, 161–172. [[CrossRef](#)]
14. Zhang, J.C.; Pu, R.L.; Wang, J.H.; Huang, W.J.; Yuan, L.; Luo, J.H. Detecting powdery mildew of winter wheat using leaf level hyperspectral measurements. *Comput. Electron. Agric.* **2012**, *85*, 13–23. [[CrossRef](#)]
15. Zhang, D.; Lin, F. Detection of wheat powdery mildew by differentiating background factors using hyperspectral imaging. *Int. J. Agric. Biol.* **2016**, *18*, 747–756. [[CrossRef](#)]
16. Feng, W.; Shen, W. Improved remote sensing detection of wheat powdery mildew using dual-green vegetation indices. *Precis. Agric.* **2016**, *17*, 608–627. [[CrossRef](#)]
17. Cao, X.; Luo, Y. Detection of powdery mildew in two winter wheat cultivars using canopy hyperspectral reflectance. *Crop Prot.* **2013**, *45*, 124–131. [[CrossRef](#)]
18. Cao, X.; Luo, Y. Detection of powdery mildew in two winter wheat plant densities and prediction of grain yield using canopy hyperspectral reflectance. *PLoS ONE* **2015**, *10*, e0121462.
19. Martens, D.A. Nitrogen cycling under different soil management systems. *Adv. Agron.* **2001**, *70*, 143–192.
20. Thomas, J.R.; Oerther, G.F. Estimating nitrogen content of sweet pepper leaves by reflectance measurements. *Agron. J.* **1972**, *64*, 11–13. [[CrossRef](#)]
21. Walburg, G.; Bauer, M.E. Effects of nitrogen nutrition on the growth, yield and reflectance characteristics of corn canopies. *Agron. J.* **1982**, *74*, 677–683. [[CrossRef](#)]
22. Yu, K.; Li, F. Remotely detecting canopy nitrogen concentration and uptake of paddy rice in the northeast China plain. *Isprs J. Photogramm.* **2013**, *78*, 102–115. [[CrossRef](#)]
23. Raun, W.R.; Johnson, G.V. Improving nitrogen use efficiency for cereal production. *Agron. J.* **1999**, *91*, 357–363. [[CrossRef](#)]
24. Hinzman, L.D.; Bauer, M.E. Effects of nitrogen fertilization on growth and reflectance characteristics of winter wheat. *Remote Sens. Environ.* **1986**, *19*, 47–61. [[CrossRef](#)]
25. Roth, G.W.; Fox, R.H. Plant-tissue tests for predicting nitrogen-fertilizer requirements of winter-wheat. *Agron. J.* **1989**, *81*, 502–507. [[CrossRef](#)]
26. Filella, I.; Serrano, L. Evaluating wheat nitrogen status with canopy reflectance indices and discriminant analysis. *Crop Sci.* **1995**, *35*, 1400–1405. [[CrossRef](#)]
27. Zhao, C.; Huang, W. The red edge parameters of different wheat varieties under different fertilization and irrigation treatments. *J. Integr. Agric.* **2002**, *1*, 745–751.
28. Hansen, P.M.; Schjoerring, J.K. Reflectance measurement of canopy biomass and nitrogen status in wheat crops using normalized difference vegetation indices and partial least squares regression. *Remote Sens. Environ.* **2003**, *86*, 542–553. [[CrossRef](#)]
29. Feng, W.; Yao, X. Monitoring leaf nitrogen status with hyperspectral reflectance in wheat. *Eur. J. Agron.* **2008**, *28*, 394–404. [[CrossRef](#)]
30. Yao, X.; Zhu, Y. Exploring hyperspectral bands and estimation indices for leaf nitrogen accumulation in wheat. *Int. J. Appl. Earth Obs.* **2010**, *12*, 89–100. [[CrossRef](#)]

31. Cui, Z.; Chen, X. On-farm evaluation of the improved soil n-based nitrogen management for summer maize in north China plain. *Agron. J.* **2008**, *100*, 517–525. [[CrossRef](#)]
32. Cao, Q.; Cui, Z. Quantifying spatial variability of indigenous nitrogen supply for precision nitrogen management in small scale farming. *Precis. Agric.* **2012**, *13*, 45–61. [[CrossRef](#)]
33. Large, E.C. Growth stages in cereals illustration of the Feekes scale. *Plant Pathol.* **1954**, *3*, 128–129. [[CrossRef](#)]
34. Sheng, B.; Duan, X. Improvement of scale 0–9 method for scoring adult plant resistance to powdery mildew of wheat. *J. Integr. Agric.* **1991**, *1*, 38–39.
35. Saari, E.E.; Prescott, J.M. A scale for appraising the foliar intensity of wheat diseases. *Plant Dis. Rep.* **1975**, *5*, 377–380.
36. Gong, P.; Pu, R. Analysis of in situ hyperspectral data for nutrient estimation of giant sequoia. *Int. J. Remote Sens.* **2002**, *23*, 1827–1850. [[CrossRef](#)]
37. Tucker, C.J. Red and photographic infrared linear combinations for monitoring vegetation. *Remote Sens. Environ.* **1979**, *8*, 127–150. [[CrossRef](#)]
38. Rouse, J.W.; Haas, R.H. Monitoring vegetation systems in the Great Plains with ERTS. In Proceedings of the Third ERTS Symposium, Washington, DC, USA, 10–14 December 1973; Volume 1, pp. 309–317.
39. Gitelson, A.A.; Kaufman, Y. Use of a green channel in remote sensing of global vegetation from EOS-MODIS. *Remote Sens. Environ.* **1996**, *58*, 289–298. [[CrossRef](#)]
40. Broge, N.H.; Leblanc, E. Comparing prediction power and stability of broadband and hyperspectral vegetation indices for estimation of green leaf area index and canopy chlorophyll density. *Remote Sens. Environ.* **2001**, *76*, 156–172. [[CrossRef](#)]
41. Haboudane, D.; Miller, J.R. Hyperspectral vegetation indices and novel algorithms for predicting green LAI of crop canopies: Modeling and validation in the context of precision agriculture. *Remote Sens. Environ.* **2004**, *90*, 337–352. [[CrossRef](#)]
42. Daughtry, C.S.; Walthall, C.L. Estimating corn leaf chlorophyll concentration from leaf and canopy reflectance. *Remote Sens. Environ.* **2000**, *74*, 229–239. [[CrossRef](#)]
43. Demetriades, S.T.H.; Steven, M.D. High resolution derivative spectra in remote sensing. *Remote Sens. Environ.* **1990**, *33*, 55–64. [[CrossRef](#)]
44. Malthus, T.J.; Maderia, A.C. High resolution spectroradiometry: Spectral reflectance of field bean leaves infected by *botrytis fabae*. *Remote Sens. Environ.* **1993**, *45*, 107–116. [[CrossRef](#)]
45. Zhu, Y.; Yao, X. Analysis of common canopy vegetation indices for indicating leaf nitrogen accumulations in wheat and rice. *Int. J. Appl. Earth Obs.* **2008**, *10*, 1–10. [[CrossRef](#)]
46. Stone, M.L.; Solie, J.B. Use of spectral radiance for correcting in-season fertilizer nitrogen deficiencies in winter wheat. *Trans. ASAE* **1996**, *39*, 1623–1631. [[CrossRef](#)]
47. Liu, W.; Cao, X.R. Detecting wheat powdery mildew and predicting grain yield using unmanned aerial photography. *Plant Dis.* **2018**, *102*, 1981–1988. [[CrossRef](#)]